# Microburst Scale Size Distribution Derived with AeroCube-6

**M. Shumko[1], T.P. O'Brien[2], J. Sample[1], A. Johnson[1], D.L. Turner[2], J.B. Blake[2], B.A. Griffith[1], O. Agapitov[3], S. Claudepierre[2]**

[1]Department of Physics, Montana State University, Bozeman, Montana, USA
[2]Space Science Applications Laboratory, The Aerospace Corportation, El Segundo, California, USA
[3]Space Sciences Laboratory, University of California berkeley, Berkeley, California, USA

**Key Points:**

- The microburst size distribution in low Earth orbit and the magnetic equator was estimated.
- In low Earth orbit the majority of microbursts have a scale size on the order of a few tens of km.
- At the magnetic equator the size of most microbursts correspond to the scale of highly correlated and high amplitude? whistler-mode chorus waves.

Corresponding author: M. Shumko, msshumko@gmail.com

**Abstract**

Microbursts are an impulsive increase of electrons from the radiation belts into the atmosphere and has been directly observed in low Earth orbit and upper atmosphere. Microburst are believed to be generated by wave-particle scattering between whistler mode waves and radiation belt electrons. Prior work has estimated that microbursts are capable of rapidly depleting the radiation belt electrons on the order of a day, hence their role to radiation belt electron losses must be considered. Radiation belt electron losses due to microbursts is not well understood, and more work is necessary to accurately quantify their contribution. To further address this question we present a statistical study of microburst scale sizes using the pair of AeroCube-6 CubeSats. The microburst scale size distribution in low Earth orbit and the magnetic equator was derived. In low Earth orbit, the majority of microbursts were found to have a size of less than a few tens of km with a minority of microbursts observed at a separation above 50 km. When mapped to the magnetic equator, the microburst scale size distribution corresponds to highly correlated and high amplitude ($> X$ pT) whistler mode chorus scale size derived in prior literature.

## 1 Plain Language Summary

https://sharingscience.agu.org/creating-plain-language-summary/

## 2 Introduction

Since the discovery of the Van Allen radiation belts in the 1960s by Van Allen (1959) and Vernov and Chudakov (1960), decades of research has made headway in understanding the dynamics particle acceleration and loss mechanisms. One of acceleration and loss mechanisms extensively studied is wave-particle scattering between whistler-mode chorus waves and electrons (Abel & Thorne, 1998; Meredith et al., 2002; Horne & Thorne, 2003; Thorne et al., 2005; Millan & Thorne, 2007; Bortnik et al., 2008). Whistler-mode chorus waves are typically generated by a temperature anisotropy of low energy electrons up to tens of kiloelectronvolts (keV) and are typically found in the $\sim 6-12$ magnetic local times (MLT) (Li, Thorne, Angelopoulos, Bortnik, et al., 2009; Li, Thorne, Angelopoulos, Bonnell, et al., 2009). Whistler-mode chorus waves interact with radiation belt electrons, and are widely believed to cause electron precipitation termed microbursts (Millan & Thorne, 2007)

Microbursts are a subsecond impulse of electrons that are observed by high altitude balloons and satellites in low Earth orbit (LEO) on the radiation belt magnetic footprints, $\sim 4-8$ L-shell (L) (Anderson & Milton, 1964; Parks, 1967; Lorentzen, Blake, et al., 2001; Lorentzen, Looper, & Blake, 2001; O'Brien et al., 2003; Woodger et al., 2015; Crew et al., 2016; Breneman et al., 2017; Mozer et al., 2018; Greeley et al., 2019). Microburst's role as a radiation belt electron loss mechanism has been estimated to be significant, with total radiation belt electron depletion due to microbursts estimated to be on the order of a day (Lorentzen, Looper, & Blake, 2001; O'Brien et al., 2004; Thorne et al., 2005; Breneman et al., 2017).

One of the unconstrained microburst parameters that is critical to better quantify the role of microbursts as a loss mechanism is their physical size. Historically there have been various case studies that estimated microburst size. Parks (1967) found that the size of mostly low energy microbursts to be $40\pm14$ km. J. Blake et al. (1996) found a microburst with a size of a few tens of km using the the Solar Anomalous and Magnetospheric Particle Explorer (SAMPEX) and concluded that typically microbursts are less than a few tens of electron gyroradii in size (order of a few km in LEO). Dietrich et al. (2010) also used SAMPEX in another case study and concluded that the observed microbursts were smaller than 4 km. More recently, Crew et al. (2016) used the Focused

Investigation of Relativistic Electron Bursts: Intensity, Range, and Dynamics (FIREBIRD-II) CubeSats and found an example of a microburst larger than 11 km, and Shumko et al. (2018) used FIREBIRD-II to identify a microburst with a size greater than $51 \pm 1$ km. The large variance in prior results imply that there is a distribution of microburst scale sizes that this study aims to estimate.

Besides addressing the microburst role in radiation belt electron losses, the microburst size distribution is pertinent to identify the wave mode(s) responsible for scattering microbursts. The microburst size distribution in LEO can be mapped to the magnetic equator and the mapped microburst size distribution compared to various wave scales derived in prior literature to identify the dominant wave properties responsible for scattering microburst electrons.

This study addresses these two questions by estimating the microburst size distribution in LEO and the magnetic equator. The twin AeroCube-6 (AC6) CubeSats are utilized for this study because they are ideally equipped for observing microbursts and they took data simultaneously over a span of three years while their separation varied between 2 and 800 km. This paper first describes the AC-6 mission, including their orbit and instrumentation. Then the procedure undertaken to identify microbursts observed by each spacecraft and how they are combined to make a list of the temporally coincident microbursts is described. Next, the microburst size distributions in LEO and the magnetic equator as a function of spacecraft separation is derived. Then a model is developed to understand how various microburst size distributions will be seen by a two-point measurement. Lastly, we discuss and summarize these results and infer the properties of the whistler-mode chorus waves that are believed to cause microbursts.

## 3 Instrumentation

The AC6 mission consists of a pair of 0.5U (10x10x5 cm) CubeSats built by the Aerospace Corporation and launched on June 19th, 2014 into a 620 x 700 km, 98 degree inclination orbit. The two satellites, designated as AC6-A and AC6-B separated after launch and drifted apart. AC6 has an active attitude control system which allows them to change their differential drag to allow fine separation control. Figure 1a shows the AC6 separation for the duration of the mission.

Each AC6 unit is equipped with a three Aerospace microdosimeters (licensed to Teledyne Microelectronics, Inc). The dosimeter used for this study is dos1 and is identical on both AC6 units. Dos1 has a 30 keV electron threshold and samples at 10 Hz. The AC6 orbit is in the dawn-dusk magnetic local times (MLTs) and Fig. 1b shows the number of good 10 Hz samples taken simultaneously by AC6 as a function and L and MLT. Good samples are samples which have a 0 data quality flag. More detailed technical information regarding the AC6 mission can be found in ? (?).

## 4 Methodology

### 4.1 Microburst Detection

The first step to find microbursts observed simultaneously by both spacecraft is to identify them from each spacecraft separately. We have detected microbursts with two different methods that yielded quantitatively similar results. The first method is the burst parameter (O'Brien et al., 2003). This algorithm has been successfully used in other microburst studies, mainly with the microbursts observed by the Solar Anomalous and Magnetospheric Particle Explorer add citations. For AC6, we found that a burst parameter threshold of 5 has good tradeoff between false positive and false negative microburst detections. Talk about the wavelet based detector as well?

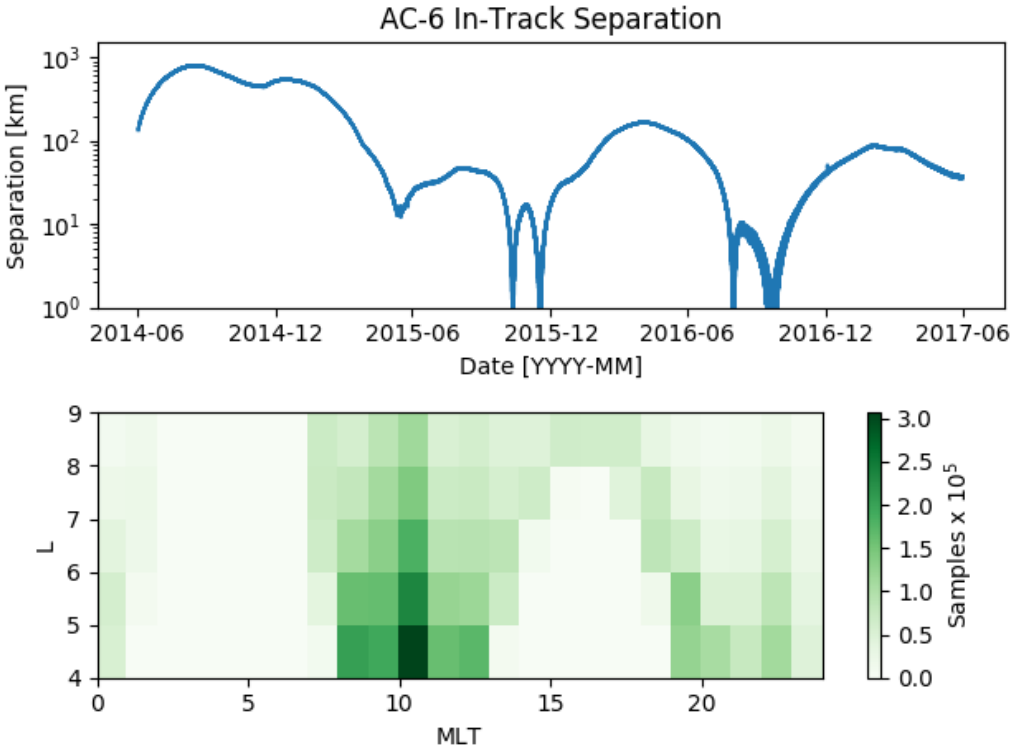


**Figure 1.** AC6 mission distributions for (a) spacecraft separation and (b) number of simltaneous 10 Hz samples as a function of L and MLT.

The transmitters on AC6 can cause unphysical count impulses in the dosimeters that resembles periodic trains of microbursts. These false detections were removed to remove their bias. One source of transmitter noise was observed at times when AC6 was in contact with the ground stations above mainland US for data downloads and commanding thus the mostly low L detections made above the US were discarded.

Another source of noise is crosslink transmissions between the AC6 units. These transmissions occurred when either spacecraft transitioned from the survey mode to 10 Hz mode. This noise is sometimes not caught by the data quality flag, so the following empirically-derived criteria was developed to remove those detections. The dosimeter with a 250 keV nominal electron threshold, dos2 was used because it had a similar response to noise while rarely responded to microbursts. Since the transmitter noise is very periodic, cross-correlation (CC) and autocorrelation (AC) methods were applied to the dos1 and dos2 time series. Detections were removed if the following two criteria were met: either dos1 or dos2 time series had a AC peak at a 0.2 or 0.4 s lag, and the dos1-dos2 CC was greater than 0.9. The AC lag criteria alone sometimes falsely removed legitimate trains of microbursts, so the second criteria insured that the detection was removed if there was a very high correlation across an order of magnitude in energy.

The lists of microbursts observed by either AC6 unit were merged into a temporally coincident list with the following procedure. Show the microburst detection cartoon I‘ve showed in conferences? The general idea is that a microburst detection on one spacecraft will CC well will the time series from the other spacecraft if it observed a similar microburst, and poorly if there was no microburst observed by the other spacecraft. Each microburst detection made by either spacecraft was CC with the time series from the other spacecraft. Windows of 1 and 1.2 s were used to CC the time series. Different window sizes were used to account for numerical uncertainty due to Poisson noise. Microbursts detections with a CC above 0.8 were considered temporally coincident. This CC threshold was chosen as it is low enough to identify temporally coincident microbursts superposed with noise, and high enough to reject most non-coincident events. Figure 2, panels (a), (c), and (e) show examples of microbursts observed by both AC6 units when they were separated by 6, 17, and 69 km, respectively.

The last CC criteria required that the temporal CC must be greater than the spatial CC + 0.3. The spatial CC was calculated by shifting the AC6-B time series by the in-track lag to CC in latitude. This criteria was applied to remove curtains, spatially stationary and narrow in latitude structures obsered by AC6 (J. B. Blake & O'Brien, 2016) and sometimes appear as microbursts. Figure 2, panels (b), (d), and (f) show the AC6 spatially aligned time series to confirm that the three cases shown were indeed microbursts. The coincident microburst list was then spot checked by two authors to any remove poorly correlated events. Considering the CC criteria and data availability, 662 confirmed simultaneous microburst detections are used to calculate the microburst scale size distribution in the following section.

### 4.2 Microburst Size Distribution in LEO and Magnetic Equator

When AC6 observes a coincident microburst at a separation $d$, the microburst‘s size must be greater than $d$. This idea is similar to Joy et al. (2002) who investigated the most probable Jovian bow shock and magnetopause standoff distances. Following the arguments presented in Section 4 in Joy et al. (2002), we investigate the dependence of the number of coincident microbursts observed above $d$, as a function of $d$ that is the microburst complementary cumulative distribution $F(d)$. If P(A) is the probability that a microburst is larger than $d$ and P(B) is the probability that AC6 is separated by $d$, then the fraction of microbursts observed at $d$ is the conditional probability $P(A \mid B)$. Using Bayes theorem,

$$P(A \mid B) = \frac{P(A \,\&\, B)}{P(B)} \tag{1}$$

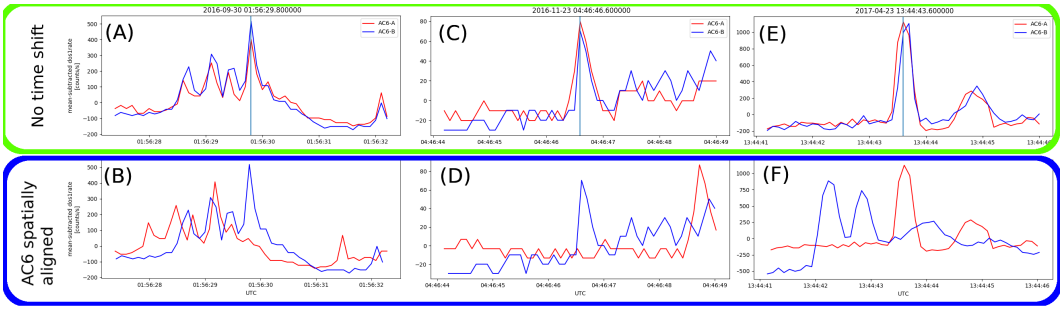


**Figure 2.** Examples of microbursts observed simulatenously by AC6. Panels (a), (c) and (e) shows the temporally-aligned time series at spacecraft separations of 5.6 km, 16.5 km, and 68.5 km, respectively. Pabels (b), (d), and (f) show the spatially aligned time series corresponding to the time series in the same column. The clear temporal correlation and lack of spatial correlation demonstrates that these events are microbursts.

where $P(A\ \&\ B)$ is the joint probability. Since the AC6 separation is independent of microburst size, $P(A\ \&\ B) = P(A)P(B)$. Hence

$$P(A \mid B) = \frac{P(A)P(B)}{P(B)} = P(A) \tag{2}$$

and seems like a big jump in logic...

$$F(d) = \frac{N(d)}{N(0)} \tag{3}$$

where $N(d)$ is the number of microbursts observed by AC6 above separation $d$ and is defined as

$$N(d) = \sum_{\text{bins>d}} n_{bin} \frac{S_{max}}{S_{bin}} \tag{4}$$

where $n_{bin}$ is the number of microbursts detected by both AC6 units in that bin. The normalization term $S_{max}/S_{bin}$ is a ratio of the number of samples observed in the most sampled bin to the number of samples in the current bin. This normalization factor corrects for AC6's non-uniform sampling in separation. With this normalization, $F(d)$ can be interpreted as the fraction of microbursts observed above $d$ assuming AC6 sampled evenly in separation. Microburst $F(d)$ in LEO is shown by the black curve in Fig. 3a for the entire radiation belt ($4 < \mathrm{L} < 8$) and split into one L-wide bins with the colored curves. The separation bin width in Fig. 3 is 5 km. To check for bias in $F(d)$ due to the separation bins, other bin widths and offsets were used to calculate $F(d)$. Bin widths as large as the size of the features in $F(d)$ (20−30 km) and bin offsets smaller than the bin width did not effect the curves in Fig. 3a.

The overall trend in Fig. 3a consists of a sudden cumulative probability drop off, followed by a shoulder up to about 70 km where the cumulative distribution drops to nearly zero. The shaded region around the black curve shows the standard error due to counting statistics. The uncertainty due to false coincidence events i.e. two unrelated microbursts randomly lining up in time was also considered. For each coincident microburst the microburst duty cycle in a one minute window ($\approx 1L$) was calculated. The false coincidence probability is then the square of the duty cycle and was found to be less than 5% for the majority of these events. The false coincidence probability for each microburst

was then used to randomly remove microbursts and $F(d)$ was recalculated in 1000 trials. The uncertainty in $F(d)$ with microbursts randomly removed was much smaller than the uncertainty due to counting statistics alone. Lastly, Fig. 3b shows the microburst probability density derived numerically from $F(d)$ and shows a peak at spacecraft separations of $d < 20$ km as well as a peak between 70-80 km.

To estimate the equatorial microburst scale size distribution, the microburst events were mapped to the magnetic equator using the Olson-Pfitzer magnetic field model (Olson & Pfitzer, 1982) which is implemneted with a Python wrapper for IRBEM-Lib (Boscher et al., 2012). Once all microburst events and spacecraft separations were mapped to the magnetic equator, the procedure to estimate $F(d)$ is identical to the LEO scale size distribution with the normalization being the only distinction. The normalization factors were calculated by mapping every AC6 time series sample taken simultaneously to the magnetic equator and binning them by separation into 100 km wide bins. Figure 4 shows the equatorial microburst scale size distribution in the same format as Fig. 3. Similar to the microburst probability density in LEO, most of the microburst probability density was observed when the AC6 equatorial separation was less than 300 km.

The results in Figs. 3 and 4 show the fraction of microbursts observed above a spacecraft separation. These measurements do not fully represent the microbursts size distribution due to the compounding effects from the range of microburst sizes and the random locations of microbursts with respect to AC6. Thus modeling is necessary to capture the influence of these statistical effects on two-point measurements.

## 5 Modeling the Microburst Size Distribution

TO-DO

- Talk about the brute force MC model.
- Show a LEO CDF model assuming a fixed-sized microburst population.
- Decide if I should show a two-fixed-sized microburst population or a microburst CDF.
- Show the residuals in the plots.

An analytic and Monte Carlo (MC) models were developed to account for the statistical effects of random microburst sizes and locations in the vicinity of AC6. FINISH THIS!

In this section we discuss the model developed to understand the relation between $F(d)$ shown in Fig. 3a and the true distribution of microburst sizes. This relation is not immediately clear since microbursts are randomly scattered around the spacecraft location during a radiation belt pass, and have an unknown geometry. We address these issues with a Monte Carlo (MC) and analytic models and we assume that microbursts are circular with a radius $r$. For simplicity we first assume that all microbursts are the same $r$ and then generalize their size to a microburst probability density function (PDF).

The MC model first randomly scattered $10^5$ microburst centers in a 400 x 400 km grid around the spacecraft. Spacecraft A is placed at the origin, and spacecraft B is placed along the positive y-axis at the same distances from the origin as the separation bins, $D$ used in Section 4.2. Then the number of simultaneously observed microbursts at each spacecraft B distance in $D$ was counted. The modeled fraction of microbursts is then

$$F(d) = \frac{\sum_{d>D} n_d}{\sum_{d \in D} n_d}. \tag{5}$$

and an example run of the MC model with a 40 km diameter microburst population is shown in Fig. 5b.

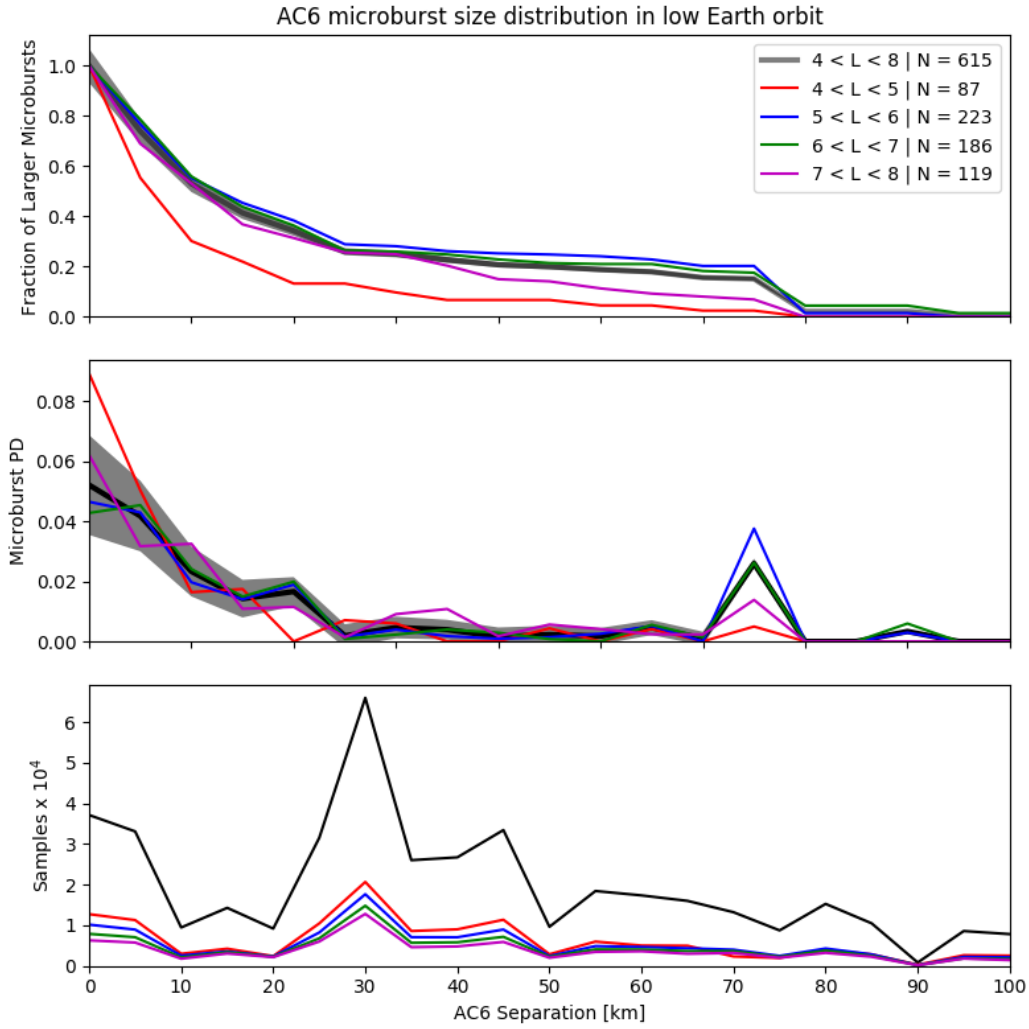


**Figure 3.** Fraction of microbursts greater than the spacecraft separation as a function of separation in LEO. Panel (a) shows the fraction of microbursts observed above that separation. Panel (b) shows the microburst probability density as a function of separation. Lastly, panel (c) shows the number of simultaneous samples AC6 observed as a function of separation. The colored lines show the distributions binned by L, and the thick black curve shows the fraction of microbursts observed above a separation in the entire radiation belt ($4 < L < 8$). The gray shading around the black curve shows the uncertainty due to counting statistics.

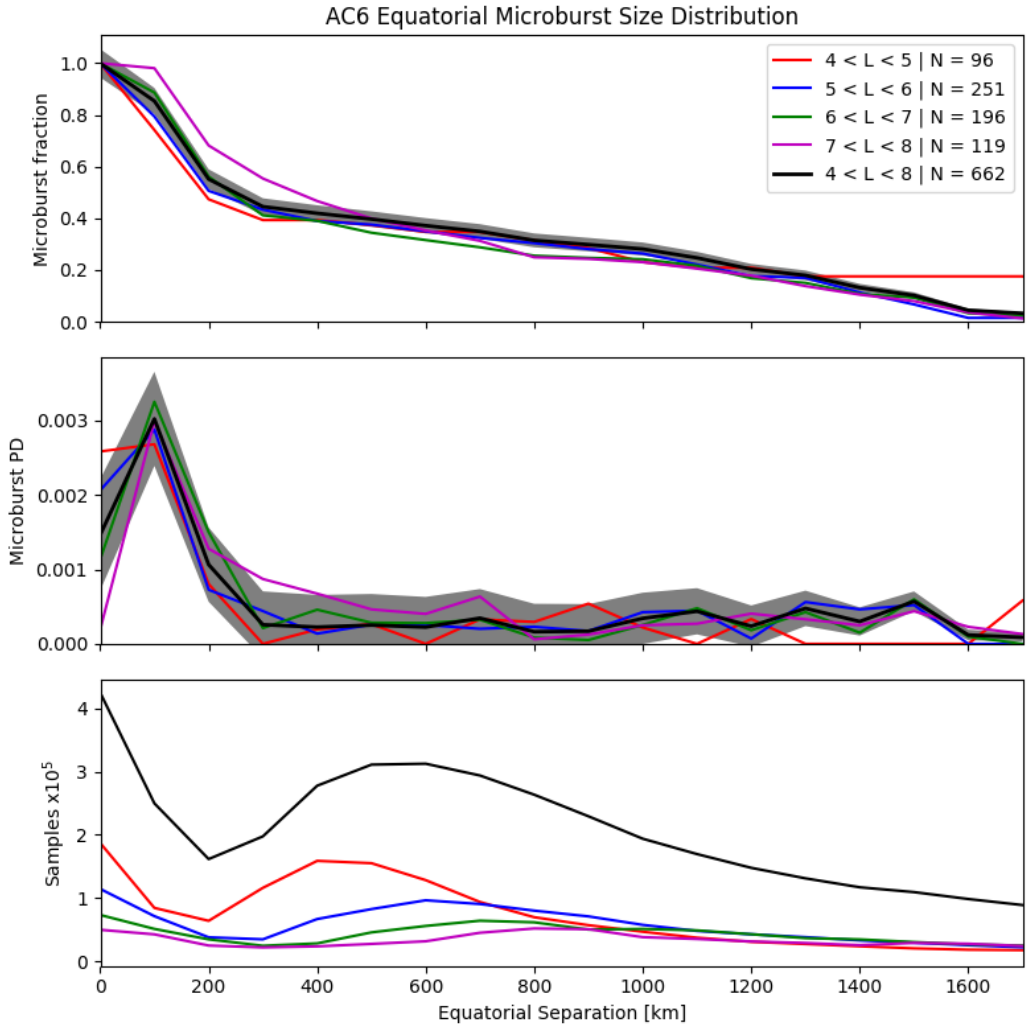


**Figure 4.** Microburst scale size distribution in the same format as Fig. 3 and mapped to the magnetic equator.

The analytic model, while identical to the MC model, highlights the concepts connecting the microburst size distribution and $F(d)$. The fundamental idea is that given a spacecraft separation $d$ and microburst radius $r$, there exists an area $A$ with the property that for any microburst center inside it will be observed by both spacecraft. The geometry of this model and $A$ is shown in Fig. 5a. Figure 5a shows the two spacecraft as blue cubes and two identical microbursts of radius $r$ shown by the black circles. This extreme case shows that the microburst centers are $r$ from either spacecraft, the maximum distance away from the spacecraft and be observed by both units. Microbursts with centers closer to the spacecraft will also be observed by both spacecraft.

Now we use the original geometry and rotate the right circle clockwise about the top spacecraft until the bottom spacecraft is outside the rotated circle. The circle's origin will trace a curve that connects the two black circle centers which is shown by the lower red-dotted line. This problem is symmetric and we can also rotate the right circle counter-clockwise about the lower spacecraft in the same manner and the center will trace out the upper red-dotted curve. The two red-dotted lines outline $A$ and if a microburst center lies anywhere in $A$, it will be observed by both spacecraft.

How do we find $A$? It must be a function of $r$ and $d$ and we need to find $A(r, d)$. Instead of tracing out the red-dotted curves between the black circles' centers, the black circles are rotated through a full revolution. This will trace out the circles comprised of the red and red-dotted curves. These centers of the two circles are separated by $d$ and the radius of the circles is $r$ and $A$ is the area where the two circles intersect and is given by

$$A(r,d) = 2r^2 \cos^{-1}\left(\frac{d}{2r}\right) - \frac{d}{2}\sqrt{4r^2 - d^2}. \tag{6}$$

Cite anything? Wolfram: http://mathworld.wolfram.com/Circle-CircleIntersection.html
Lastly, the fraction of microbursts as a function of separation is given by

$$F(r,d) = \frac{\sum_{d>D} A(r,d)}{\sum_{d\in D} A(r,d)}. \tag{7}$$

Where the denominator is the normalization factor. An example of the analytic $F(r = 20\text{ km}, d)$ is shown in Fig. 5b with the dashed blue curve.

## 6 Discussion

TO-DO

- Discuss the significance of the peaks in the LEO CDF & PDF.
- Discuss the secondary peak.
- Talk about how these sizes fit in with prior work and how they can be used to estimate microburst loss rates.
- Maybe add a plot with Oleksiy's data?
- Use the wave data to interpret the equatorial scale size distribution. Is the ¡ 200 km peak due to high amplitude waves, or is it just that waves are most common at those scales?

## 7 Conclusions

**Acknowledgments**
Enter acknowledgments, including your data availability statement, here.

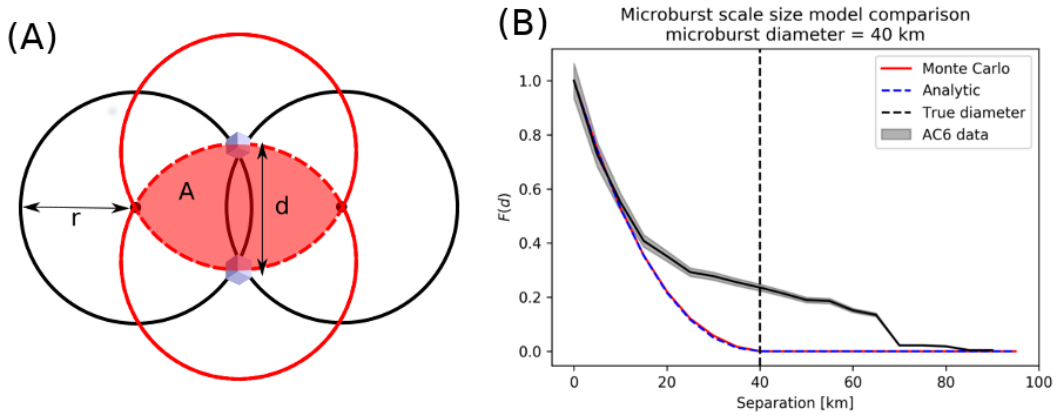


**Figure 5.** Modeling a single-sized microburst distribution. Panel A shows the geometry of the analytic model. Assuming a microburst radius $r$ (microbursts shown with black circles) and spacecraft separation $d$, the area $A$ shows all possible microburst center locations where a microburst will be simultaneously observed by both spacecraft. The two black circles show the most distant microburst location that is observed by both spacecraft. The red solid and dashed curves are found by rotating either of the black circles about the top and bottom spacecraft. Panel B shows the microburst fraction, $F(d)$ as a function of separation from the AC6 data in solid black. The red and dashed blue curves show the $F(d)$ assuming all microbursts have a 40 km diameter.

## References


Abel, B., & Thorne, R. M. (1998). Electron scattering loss in earth's inner magnetosphere: 1. dominant physical processes. *Journal of Geophysical Research: Space Physics*, *103*(A2), 2385–2396.

Anderson, K. A., & Milton, D. W. (1964). Balloon observations of X rays in the auroral zone: 3. High time resolution studies. *Journal of Geophysical Research*, *69*(21), 4457–4479. Retrieved from `http://dx.doi.org/10.1029/JZ069i021p04457` doi: 10.1029/JZ069i021p04457

Blake, J., Looper, M., Baker, D., Nakamura, R., Klecker, B., & Hovestadt, D. (1996). New high temporal and spatial resolution measurements by sampex of the precipitation of relativistic electrons. *Advances in Space Research*, *18*(8), 171 - 186. Retrieved from `http://www.sciencedirect.com/science/article/pii/0273117795009698` doi: http://dx.doi.org/10.1016/0273-1177(95)00969-8

Blake, J. B., & O'Brien, T. P. (2016). Observations of small-scale latitudinal structure in energetic electron precipitation. *Journal of Geophysical Research: Space Physics*, *121*(4), 3031–3035. Retrieved from `http://dx.doi.org/10.1002/2015JA021815` (2015JA021815) doi: 10.1002/2015JA021815

Bortnik, J., Thorne, R., & Inan, U. S. (2008). Nonlinear interaction of energetic electrons with large amplitude chorus. *Geophysical Research Letters*, *35*(21).

Boscher, D., Bourdarie, S., O'Brien, P., Guild, T., & Shumko, M. (2012). *Irbem-lib library.*

Breneman, A., Crew, A., Sample, J., Klumpar, D., Johnson, A., Agapitov, O., ... others (2017). Observations directly linking relativistic electron microbursts to whistler mode chorus: Van allen probes and FIREBIRD II. *Geophysical Research Letters*.

Crew, A. B., Spence, H. E., Blake, J. B., Klumpar, D. M., Larsen, B. A., O'Brien, T. P., ... Widholm, M. (2016). First multipoint in situ observations of elec-

tron microbursts: Initial results from the NSF FIREBIRD II mission. *Journal of Geophysical Research: Space Physics*, *121*(6), 5272–5283. Retrieved from http://dx.doi.org/10.1002/2016JA022485 (2016JA022485) doi: 10.1002/2016JA022485

Dietrich, S., Rodger, C. J., Clilverd, M. A., Bortnik, J., & Raita, T. (2010). Relativistic microburst storm characteristics: Combined satellite and ground-based observations. *Journal of Geophysical Research: Space Physics*, *115*(A12).

Greeley, A., Kanekal, S., Baker, D., Klecker, B., & Schiller, Q. (2019). Quantifying the contribution of microbursts to global electron loss in the radiation belts. *Journal of Geophysical Research: Space Physics*.

Horne, R. B., & Thorne, R. M. (2003). Relativistic electron acceleration and precipitation during resonant interactions with whistler-mode chorus. *Geophysical Research Letters*, *30*(10). Retrieved from http://dx.doi.org/10.1029/2003GL016973 (1527) doi: 10.1029/2003GL016973

Joy, S., Kivelson, M., Walker, R., Khurana, K., Russell, C., & Ogino, T. (2002). Probabilistic models of the jovian magnetopause and bow shock locations. *Journal of Geophysical Research: Space Physics*, *107*(A10), SMP–17.

Li, W., Thorne, R., Angelopoulos, V., Bonnell, J., McFadden, J., Carlson, C., ... Auster, H. (2009). Evaluation of whistler-mode chorus intensification on the nightside during an injection event observed on the THEMIS spacecraft. *Journal of Geophysical Research: Space Physics*, *114*(A1).

Li, W., Thorne, R. M., Angelopoulos, V., Bortnik, J., Cully, C. M., Ni, B., ... Magnes, W. (2009). Global distribution of whistler-mode chorus waves observed on the THEMIS spacecraft. *Geophysical Research Letters*, *36*(9). Retrieved from http://dx.doi.org/10.1029/2009GL037595 (L09104) doi: 10.1029/2009GL037595

Lorentzen, K. R., Blake, J. B., Inan, U. S., & Bortnik, J. (2001). Observations of relativistic electron microbursts in association with VLF chorus. *Journal of Geophysical Research: Space Physics*, *106*(A4), 6017–6027. Retrieved from http://dx.doi.org/10.1029/2000JA003018 doi: 10.1029/2000JA003018

Lorentzen, K. R., Looper, M. D., & Blake, J. B. (2001). Relativistic electron microbursts during the GEM storms. *Geophysical Research Letters*, *28*(13), 2573–2576. Retrieved from http://dx.doi.org/10.1029/2001GL012926 doi: 10.1029/2001GL012926

Meredith, N., Horne, R., Summers, D., Thorne, R., Iles, R., Heynderickx, D., & Anderson, R. (2002). Evidence for acceleration of outer zone electrons to relativistic energies by whistler mode chorus. In *Annales geophysicae* (Vol. 20, pp. 967–979).

Millan, R., & Thorne, R. (2007). Review of radiation belt relativistic electron losses. *Journal of Atmospheric and Solar-Terrestrial Physics*, *69*(3), 362 - 377. Retrieved from //www.sciencedirect.com/science/article/pii/S1364682606002768 doi: http://dx.doi.org/10.1016/j.jastp.2006.06.019

Mozer, F. S., Agapitov, O. V., Blake, J. B., & Vasko, I. Y. (2018). Simultaneous observations of lower band chorus emissions at the equator and microburst precipitating electrons in the ionosphere. *Geophysical Research Letters*. Retrieved from http://dx.doi.org/10.1002/2017GL076120 doi: 10.1002/2017GL076120

O'Brien, T. P., Looper, M. D., & Blake, J. B. (2004). Quantification of relativistic electron microburst losses during the GEM storms. *Geophysical Research Letters*, *31*(4). Retrieved from http://dx.doi.org/10.1029/2003GL018621 (L04802) doi: 10.1029/2003GL018621

O'Brien, T. P., Lorentzen, K. R., Mann, I. R., Meredith, N. P., Blake, J. B., Fennell, J. F., ... Anderson, R. R. (2003). Energization of relativistic electrons in the presence of ULF power and MeV microbursts: Evidence for dual ULF and VLF acceleration. *Journal of Geophysical Research: Space Physics*,

*108*(A8). Retrieved from http://dx.doi.org/10.1029/2002JA009784 doi: 10.1029/2002JA009784

Olson, W. P., & Pfitzer, K. A. (1982). A dynamic model of the magnetospheric magnetic and electric fields for july 29, 1977. *Journal of Geophysical Research: Space Physics*, *87*(A8), 5943–5948. Retrieved from http://dx.doi.org/10.1029/JA087iA08p05943 doi: 10.1029/JA087iA08p05943

Parks, G. K. (1967). Spatial characteristics of auroral-zone X-ray microbursts. *Journal of Geophysical Research*, *72*(1), 215–226.

Shumko, M., Sample, J., Johnson, A., Blake, B., Crew, A., Spence, H., ... Handley, M. (2018). Microburst scale size derived from multiple bounces of a microburst simultaneously observed with the firebird-ii cubesats. *Geophysical Research Letters*, *45*(17), 8811-8818. Retrieved from https://agupubs.onlinelibrary.wiley.com/doi/abs/10.1029/2018GL078925 doi: 10.1029/2018GL078925

Thorne, R. M., O'Brien, T. P., Shprits, Y. Y., Summers, D., & Horne, R. B. (2005). Timescale for MeV electron microburst loss during geomagnetic storms. *Journal of Geophysical Research: Space Physics*, *110*(A9). Retrieved from http://dx.doi.org/10.1029/2004JA010882 (A09202) doi: 10.1029/2004JA010882

Van Allen, J. A. (1959). The geomagnetically trapped corpuscular radiation. *Journal of Geophysical Research*, *64*(11), 1683–1689. Retrieved from http://dx.doi.org/10.1029/JZ064i011p01683 doi: 10.1029/JZ064i011p01683

Vernov, S., & Chudakov, A. (1960). Investigation of radiation in outer space. In *International cosmic ray conference* (Vol. 3, p. 19).

Woodger, L., Halford, A., Millan, R., McCarthy, M., Smith, D., Bowers, G., ... Liang, X. (2015). A summary of the BARREL campaigns: Technique for studying electron precipitation. *Journal of Geophysical Research: Space Physics*, *120*(6), 4922–4935.